Optimized mid-infrared thermal emitters for applications in aircraft countermeasures

Simón G. Lorenzo, Chenglong You, Christopher H. Granier, Georgios Veronis, and Jonathan P. Dowling

Citation: AIP Advances **7**, 125112 (2017);
View online: https://doi.org/10.1063/1.5003800
View Table of Contents: http://aip.scitation.org/toc/adv/7/12
Published by the American Institute of Physics

Optimized mid-infrared thermal emitters for applications in aircraft countermeasures

Simón G. Lorenzo,[1,a] Chenglong You,[1] Christopher H. Granier,[1] Georgios Veronis,[2,3] and Jonathan P. Dowling[1]
[1]*Hearne Institute for Theoretical Physics and Department of Physics and Astronomy, Louisiana State University, Baton Rouge, Louisiana 70803, USA*
[2]*Center for Computation and Technology, Louisiana State University, Baton Rouge, Louisiana 70803, USA*
[3]*School of Electrical Engineering and Computer Science, Louisiana State University, Baton Rouge, Louisiana 70803, USA*

(Received 7 September 2017; accepted 4 December 2017; published online 13 December 2017)

We introduce an optimized aperiodic multilayer structure capable of broad angle and high temperature thermal emission over the 3 μm to 5 μm atmospheric transmission band. This aperiodic multilayer structure composed of alternating layers of silicon carbide and graphite on top of a tungsten substrate exhibits near maximal emittance in a 2 μm wavelength range centered in the mid-wavelength infrared band traditionally utilized for atmospheric transmission. We optimize the layer thicknesses using a hybrid optimization algorithm coupled to a transfer matrix code to maximize the power emitted in this mid-infrared range normal to the structure's surface. We investigate possible applications for these structures in mimicking 800–1000 K aircraft engine thermal emission signatures and in improving countermeasure effectiveness against hyperspectral imagers. We find these structures capable of matching the Planck blackbody curve in the selected infrared range with relatively sharp cutoffs on either side, leading to increased overall efficiency of the structures. Appropriately optimized multilayer structures with this design could lead to matching a variety of mid-infrared thermal emissions. For aircraft countermeasure applications, this method could yield a flare design capable of mimicking engine spectra and breaking the lock of hyperspectral imaging systems. https://doi.org/10.1063/1.5003800

I. INTRODUCTION

Infrared countermeasures break or jam seeker-missile signal locks on fixed-wing or rotor aircraft. The first infrared seeker missiles utilized a simple spinning wheel reticle in front of an infrared sensor to generate a pulsed target signal.[1,2] The phase shift in this signal as the target or missile deviated spatially triggered servo-motors in the fins and adjusted the missile's trajectory.[1] Aircraft are uniquely susceptible to spectrum-seeking devices due to their engine emissions' high spectral contrast with the atmospheric background.

Initially, simple aircraft-mounted flares functioned to divert seeker missiles through highly exothermic reactions that obscured the aircraft's spectral signature.[3] Conventional flares largely fall into the categories of magnesium/teflon/viton (MTV) flares, or solid-liquid pyrophoric countermeasures. Typical MTV flares burn at approximately 2300 K with unique combustion peaks, and pyrophoric countermeasures in both states operate similarly at high temperatures. These countermeasures also have high energy rises upon ignition.[4]

Seeker missiles developed rapidly in complexity, utilizing complex rosette reticle patterns, reflecting mirrors, and more robust signal analysis methods to prevent a lock-on break with the

[a]Electronic mail: slorenzo6314@gmail.com

target.[1,2] Aircraft can use a combination of infrared signal jammers and high-volume flare ejections to counter some of these new advanced threats.

However, modern missiles identify multiple target emission characteristics and resist these countermeasures, posing a danger to modern pilots.[1] Seeker missiles using spectrum rise analysis discern steady-spectra aircraft engine components from high-rise flare signatures. The spectrum for aircraft engines is dominated by the combustion plume and the engine components near the exhaust.[3] Combined, these effects peak in the mid-infrared atmospheric transmission band (3–5 μm), characteristic of Planck blackbody emission for 800–1000 K. Hyperspectral imagers mounted on missiles can discern these lower temperature aircraft spectra from 2300 K flares through comparison of emission intensities over various wavelengths.

A high-intensity emitter mimicking a low-rise 800–1000 K aircraft emission spectrum could successfully break the aircraft lock of these countermeasure-resistant missiles. In this paper, we propose one-dimensional multilayer aperiodic structures heated by an internal resistive element. It has been shown that optimized multilayered structures exhibit properties similar to more complex and harder-to-fabricate two- or three-dimensional structures.[5] Here, we optimize the layer thicknesses using a transfer-matrix code[6] to maximize the power emitted in the 3–5 μm wavelength range in the normal direction. This wavelength range corresponds to both the mid-infrared atmospheric transmission window and the combined aircraft engine and fuel combustion spectra. The proposed structure consists of silicon carbide, graphite, and tungsten with melting points well above the 800–1000 K aircraft engine exterior temperatures.[3] For practical applications, the structure should be coated in a protective material to prevent graphite oxidization at high temperatures.

Similar broadband thermal absorbers and emitters have been successfully researched for applications in solar thermophotovoltaics,[7,8] incandescent lighting,[9] energy conversion,[10] and electro-optical detectors.[11] However, these are typically applications in the visible to near infrared range and largely ignore the mid-infrared atmospheric transmission windows.[3]

II. THEORY

We model a structure composed of materials of infinite width and length but with varying aperiodic thicknesses above a semi-infinite tungsten base as depicted in Fig. 1. Using the transfer matrix method, we calculate structure transmittance, reflectance, and absorptance for TE and TM polarizations.[6] We note that the transfer matrix method is exact for one-dimensional multilayer structures. We also note that we have extensively validated our transfer matrix code by comparing its results with results obtained with other numerical methods such as the finite-difference frequency-domain method. We model the structure in vacuum (approximately air) with emitted light measured at an angle θ from the surface normal. We make use of experimental data for the wavelength-dependent

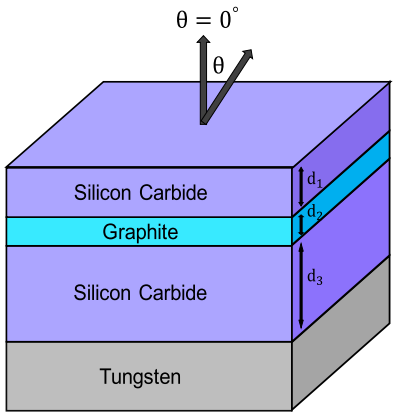

FIG. 1. Schematic of the structure optimized by genetic algorithm coupled to the transfer matrix code. Emitted light at an angle θ to the surface normal of the structure exits the three-layer alternating structure of silicon carbide and graphite above a semi-infinite tungsten substrate.

indices of refraction, both real and imaginary parts, for silicon carbide, graphite, and tungsten.[12–14] We choose these materials for their melting points above 2500 K[15] as required for stable 800–1000 K thermal emitters. The semi-infinite tungsten substrate reduces transmittance to zero so that,

$$A(\lambda, \theta) = 1 - R(\lambda, \theta), \tag{1}$$

where A is the absorptance, R is the reflectance, and λ is the wavelength. We use Kirchoff's second law and energy conservation to equate absorptance A and emittance ϵ under thermal equilibrium.[16]

The power radiated per unit area and wavelength is given by Planck blackbody spectrum (in units of Watts per square meter per nanometer),

$$B(\lambda, T) = \frac{2hc^2}{\lambda^5}[\exp(\frac{hc}{\lambda k_B T}) - 1]^{-1}, \tag{2}$$

where h is Planck's constant, c is the speed of light, λ is wavelength, T is the temperature, and k_B is the Boltzmann constant. We define normalized power radiated per unit area per unit wavelength $\mu(\lambda, \theta)$ by the structure as the ratio of total radiated power to the maximum power found at the Wien wavelength for that temperature,

$$\mu(\lambda, \theta) = \frac{\epsilon_{\text{Total}}(\lambda, \theta)B(\lambda, T = 900\text{ K})}{\max_\lambda [B(\lambda, T = 900\text{ K})]}, \tag{3}$$

where

$$\epsilon_{\text{Total}}(\lambda, \theta) = \frac{\epsilon_{TE}(\lambda, \theta) + \epsilon_{TM}(\lambda, \theta)}{2}. \tag{4}$$

We define the efficiency of a given structure as the ratio of normalized power emitted in the desired wavelength range in the normal direction to the total power emitted,

$$\eta = \frac{\int_{\lambda_1}^{\lambda_2} \mu(\lambda, \theta = 0^\circ)d\lambda}{\int_0^\infty \mu(\lambda, \theta = 0^\circ)d\lambda}. \tag{5}$$

We choose an operating temperature of 900 K with a Wien wavelength of ~3.22 μm, corresponding to the 3–5 μm mid-infrared atmospheric transmission band and the typical range of aircraft operating temperatures (800–1000 K).[3]

III. RESULTS

We are interested in matching a specific emission spectrum in the 3–5 μm atmospheric window.[3] As a proof of concept, however, we first search for a structure capable of plateau-like unity emittance (ϵ=1), across this mid-infrared wavelength range with minimal emittance (ϵ=0) outside of that range (the solid green line in Fig. 2).

We use a hybrid optimization method consisting of a microgenetic global optimization algorithm[17–22] coupled to a local optimization algorithm[23] to determine the best dimensions for multilayered structures on top of the semi-infinite substrate. The genetic algorithm is an iterative optimization procedure that begins with a randomly selected population of potential structure dimensions and evolves toward improved solutions as defined by the selected fitness function. Once the population converges, the local optimization algorithm finds the local optimum. The process retains the best structure and is iteratively repeated for a set number of generations.

Specifically, we first maximize the fitness function F_1:

$$F_1 = \int_{\lambda_1}^{\lambda_2} \mu(\lambda, \theta = 0^\circ)d\lambda, \tag{6}$$

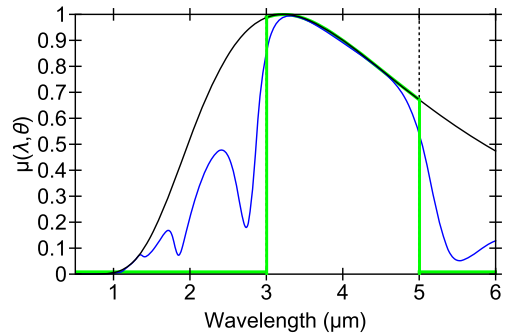

FIG. 2. Normalized power emitted per unit area and unit wavelength in the normal direction, $\mu(\lambda, \theta = 0^\circ)$ as a function of wavelength by a blackbody (black), an ideal emitter (green), and the proposed optimized emitter structure of Fig. 1 (blue). Each is calculated at a temperature of 900 K (below the melting point of all structure materials) and normalized by the power emitted by a blackbody at the 3.2 μm peak emission wavelength for a 900 K blackbody. The dashed vertical gray lines indicate the 3–5 μm wavelength region of interest for infrared emission. The layer thicknesses of the optimized silicon-carbide and graphite structure of Fig. 1 in units of nanometers, beginning with the silicon carbide layer bordering air, are {337, 75.5, 1000}.

where λ_1 and λ_2 are the respective lower and upper wavelength bounds on the calculation of the emitted power in the wavelength range of interest (in our case λ_1=3 μm and λ_2=5 μm). This process is carried out to enhance the emittance in the mid-infrared range.

We then seek to maximize the efficiency of the structure without significantly decreasing the enhancement of the power emitted in the mid-infrared. Thus, we minimize the normalized power emitted by the structure, F_2,

$$F_2 = \int_0^\infty \mu(\lambda, \theta = 0^\circ) d\lambda, \tag{7}$$

subject to the constraint that the fitness function F_1 for the structure is at least 98% of the previously calculated maximum F_1.

We consider structures of three layers composed of alternating silicon carbide and graphite layers above a semi-infinite tungsten substrate (henceforth referred to as the SiC-C structure) (Fig. 2). We found that using more than three layers leads to negligible structure improvement. The optimized structure with dimensions outlined in Fig. 2 shows near maximal emittance in the 3–5 μm region in a broad angular range out to ~50° (Fig. 3). Additionally, narrow bands of broad-angle close-to-unity emittance exist closer to the visible. While negligible when calculating the output power, these narrow

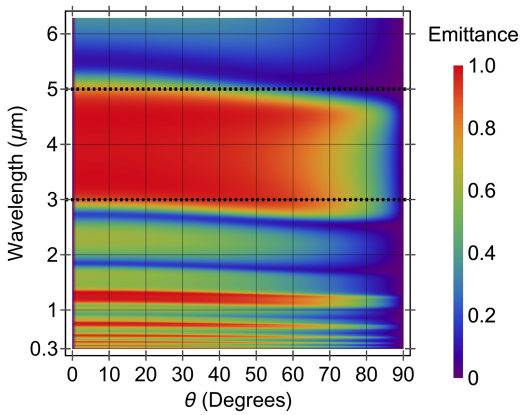

FIG. 3. Emittance as a function of wavelength and angle for the genetic algorithm-optimized structure described in Fig. 1. The horizontal, dashed, black lines show the 3–5 μm wavelength optimization range. The layer thicknesses are as given in Fig. 2.

lines indicate the versatility of the proposed aperiodic multilayer structures in both broad and narrow wavelength infrared emission applications.

When multiplied by the wavelength-dependent emittance of a blackbody spectrum for 900 K, the structure tracks the blackbody curve in the 3–5 μm band with decreased power outside this atmospheric transmission range (Fig. 2). This shows that a multilayer SiC-C structure on a tungsten substrate can be optimized for maximum emission in the 3–5 μm atmospheric transmission range with power values matching the blackbody curve for 900 K. While the efficiency of emission in the

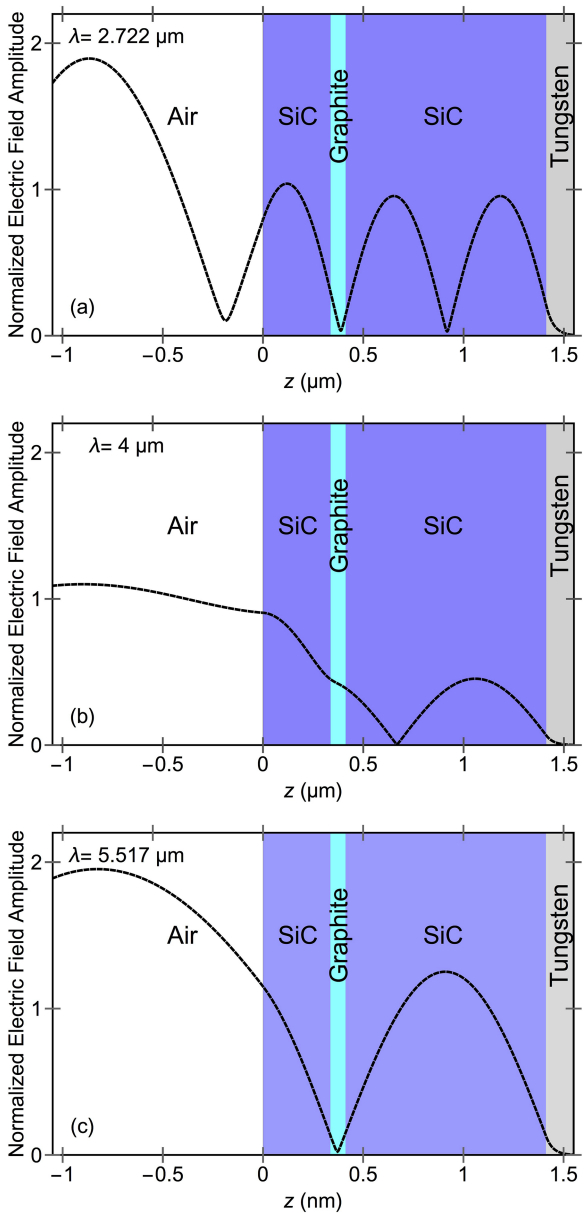

FIG. 4. Profile of the electric field amplitude, normalized with respect to the field amplitude of the incident plane wave for the genetic-algorithm-optimized structure described in Fig. 2. (a) The structure is excited by a normally incident plane wave at a minimal emittance wavelength of $\lambda = 2.722\mu$m. (b) The structure is excited by a normally incident plane wave at a maximal emittance wavelength of $\lambda = 4\mu$m. The ratio of power absorbed inside each layer to the total power absorbed in the structure from left to right beginning with the layer adjacent to air is $\{0, 0.993, 0, 0.007\}$. That is, 99.3% of the total power absorbed is absorbed in the SiC layer, while 0.7% is absorbed in the tungsten substrate. (c) The structure is excited by a normally incident plane wave at a minimal emittance wavelength of $\lambda = 5.517\mu$m. The structural layer thicknesses are as given in Fig. 2.

3–5 μm range (defined above) will depend heavily on the operating temperature in accordance with the blackbody curve, it was calculated to be ~72.3% for the structure heated to 900 K. We note that the sidelobes in the emittance outside the 3–5 μm wavelength region of interest could be reduced through apodization of the multilayer structures.[24,25]

In Fig. 4 we show the profiles of the electric field amplitude normalized with respect to the field amplitude of incident plane waves for the optimized structure. The structure is excited by normally incident plane waves at the characteristically minimal and maximal power output wavelengths of 2.722 μm, 4 μm, and 5.517 μm as seen in Fig. 2. For the 4 μm wavelength characteristic of maximal emission, we see in Fig. 4(b) that high absorption in the lossy graphite layer is preferable to absorption in the tungsten substrate. This structure can lead to high emittance at 4 μm, because it can provide almost perfect impedance matching between air and the tungsten substrate. The wave impedance $\eta_{\mathrm{A,\,B}}$ of a uniform layer A upon a substrate B is obtained using the impedance transformation

$$\eta_{\mathrm{A,B}} = \eta_{\mathrm{A}} \frac{\eta_{\mathrm{B}} + \eta_A \tanh(\gamma_{\mathrm{A}} d_{\mathrm{A}})}{\eta_{\mathrm{A}} + \eta_{\mathrm{B}} \tanh(\gamma_{\mathrm{A}} d_{\mathrm{A}})}, \tag{8}$$

where η_{A} and η_{B} are the impedances of the material in the layer and the substrate, respectively; d_A is the thickness of A; and $\gamma_A = i\omega(\mu\epsilon)^{1/2}$, where ω is the angular frequency, μ is the dielectric permeability, and ϵ is the dielectric permittivity of the layer. Using this equation repeatedly for each layer, an impedance value of $\eta_{\mathrm{structure}} = (310.6 + 19.9\mathrm{i})\ \Omega$ at 4 μm is obtained for the overall structure compared to η_{air} =376.7 Ω. This corresponds to a structural power reflection coefficient of ~0.01 and emittance of ~0.99, where the power reflection coefficient is R=$|r|^2$ and

$$r = \frac{\eta_{\mathrm{air}} - \eta_{\mathrm{structure}}}{\eta_{\mathrm{air}} + \eta_{\mathrm{structure}}}. \tag{9}$$

Alternatively, low field intensity in the graphite layer results in low mid-infrared emission and high reflection for the structure at 2.722 μm and 5.517 μm [Figs. 4(a) and 4(c)]. At these wavelengths of minimum emission, the field has a node in the graphite layer and tungsten substrate, corresponding to a Fabry-Perot cavity in the silicon carbide layer adjacent to the substrate of one and half a wavelength, respectively. The power reflection coefficients at 2.722 μm, 4 μm, and 5.517 μm are 0.80, 0.10, and 0.91, respectively. There is also no field enhancement within the structure. Therefore, the high emittance is not associated with resonant field enhancement in the structure, as indicated by the broad wavelength and angular characteristics.

We also investigate the effects of individual layer thicknesses on the emittance spectrum of the SiC-C structure (Fig. 5). The optimal thickness for the SiC layer adjacent to air for 3–5 μm broad wavelength emission is 337 nm [Fig. 5(a)]. Similarly, the graphite layer exhibits high structural emittance contributions for thicknesses between 30 and 140 nm for the 3–5μm wavelength range [Fig. 5(b)]. The optimal layer thickness here is 75.5 nm. Finally, the wavelength range of close-to-unity emittance for the structure of Fig. 1 is tunable through the layer thickness of the SiC layer

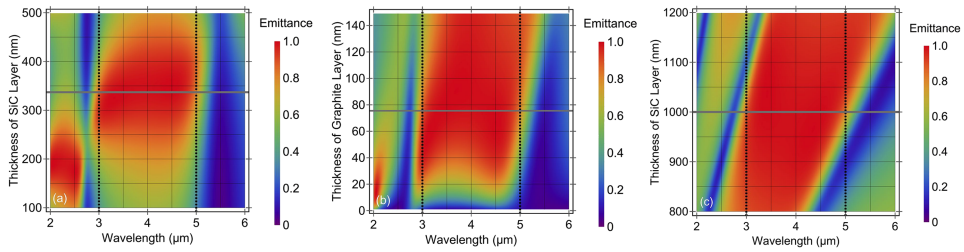

FIG. 5. (a) Emittance in the normal direction as a function of wavelength and the thickness of the first silicon carbide layer adjacent to air. All other layer thicknesses are as in the optimized structure described in Fig. 2. (b) Emittance in the normal direction as a function of wavelength and the thickness of the graphite layer below the silicon-carbide layer. All other layer thicknesses are as in the optimized structure described in Fig. 2. (c) Emittance in the normal direction as a function of wavelength and the thickness of the silicon-carbide layer below the graphite layer. All other layer thicknesses are as in the optimized structure described in Fig. 2. The vertical, dashed, black lines indicate the 3–5 μm wavelength range, while the solid horizontal grey lines indicate the optimized structure dimensions as given in Fig. 2.

adjacent to the substrate [Fig. 5(c)]. For the 3–5 μm range, the optimal thickness lies at the 1000 nm thickness used in our structure. We note that close-to-unity emittance at 4 μm wavelength can also be achieved for a smaller layer thickness of ~200 nm. However, for such thickness the high emittance wavelength range is much broader, so that the efficiency of the structure [Eq. (5)] is significantly lower than the one of the optimized structure. For all of these layers, the broad dimensional tolerances indicate robustness in structural design.

Considering the dimensional tolerances in the optimized structure, linear thermal expansion in the normal direction to the structure surface would lead to negligible changes in the emittance of the structure. Graphite, silicon carbide, and tungsten have linear thermal expansion coefficients for 900 K of $\sim 8 \times 10^{-6}$ K^{-1}, $\sim 5 \times 10^{-6}$ K^{-1} and $\sim 4.3 \times 10^{-6}$ K^{-1}, respectively.[26] The linear thermal expansions for each layer at 900 K in units of nanometers are (SiC: 1.5, C: 0.5, SiC: 4.5), and, considering the results of Fig. 5, fall well within the dimensional tolerances of each structural layer.

IV. CONCLUSION

We designed a thin-film structure composed of alternating layers of silicon carbide and graphite of aperiodic thicknesses above a semi-infinite tungsten substrate. We used a hybrid optimization algorithm consisting of a global stochastic micro-genetic algorithm coupled to a local deterministic algorithm to optimize structural dimensions for maximum emitted power in the 3–5 μm wavelength range. We then minimized the power emitted outside this atmospheric transmission window without appreciably reducing the emitted power in the wavelength region of interest. The optimized structures exhibit near-maximal 900 K blackbody emission across the 3–5μm range and at angles up to ~50° from the surface normal. Over this range, the structure exhibits almost perfect impedance matching to air without any associated field enhancement.

We showed that thermal emitters heated to the typical aircraft operating temperatures can exhibit high selective power output in the 3–5 μm atmospheric transmission window. Typical aircraft exhaust and engine component spectra also peak in this wavelength range. Investigation of the structure's layers dimensional tolerances indicates a robust design facilitating fabrication. The tungsten substrate could be heated as a resistor using current supplied by an internal battery. For countermeasure applications with specific aircraft spectra provided, this optimization method could yield a flare design capable of mimicking engine spectra and breaking the lock of hyperspectral imaging systems.

ACKNOWLEDGMENTS

S. G. Lorenzo and J. P. Dowling would like to acknowledge support from the Air Force Office of Scientific Research, the Army Research Office, the National Science Foundation, and the Northrop Grumman corporation. C. You would like to acknowledge support from an Economic Development Assistantship from the Louisiana State University System Board of Regents. G. Veronis acknowledges support from the National Science Foundation (award number 1254934). All the authors would like to acknowledge interesting and useful discussions with Jason Ralph.

[1] R. E. Ball, *The Fundamentals of Aircraft Combat Survivability Analysis and Design* (AIAA American Institute of Aeronautics & Astronautics, 2003).
[2] R. G. Driggers, C. E. Halford, G. D. Boreman, D. Lattman, and K. F. Williams, "Parameters of spinning FM reticles," Appl. Opt. **30**, 887–895 (1991).
[3] J. R. White, "Aircraft infrared principles, signatures, threats, and countermeasures," Tech. Rep. (DTIC Document, 2012).
[4] E.-C. Koch, "Pyrotechnic countermeasures: II. Advanced aerial infrared countermeasures," Propellants Explos. Pyrotech. **31**, 3–19 (2006).
[5] W. Wang, Y. Cui, Y. He, Y. Hao, Y. Lin, X. Tian, T. Ji, and S. He, "Efficient multiband absorber based on one-dimensional periodic metal–dielectric photonic crystal with a reflective substrate," Opt. Lett. **39**, 331–334 (2014).
[6] C. M. Cornelius and J. P. Dowling, "Modification of Planck blackbody radiation by photonic band-gap structures," Phys. Rev. A **59**, 4736 (1999).
[7] J. Fleming, S. Lin, I. El-Kady, R. Biswas, and K. Ho, "All-metallic three-dimensional photonic crystals with a large infrared bandgap," Nat. **417**, 52–55 (2002).
[8] M. Florescu, H. Lee, I. Puscasu, M. Pralle, L. Florescu, D. Z. Ting, and J. P. Dowling, "Improving solar cell efficiency using photonic band-gap materials," Sol. Energy Mater. Sol. Cells **91**, 1599–1610 (2007).
[9] C. H. Granier, S. G. Lorenzo, C. You, G. Veronis, and J. P. Dowling, "Optimized aperiodic broadband visible absorbers," J. Opt. (2017).

[10] Y. Cui, Y. He, Y. Jin, F. Ding, L. Yang, Y. Ye, S. Zhong, Y. Lin, and S. He, "Plasmonic and metamaterial structures as electromagnetic absorbers," Laser Photon. Rev. **8**, 495–520 (2014).
[11] A. Polman and H. A. Atwater, "Photonic design principles for ultrahigh-efficiency photovoltaics," Nat. Mater. **11**, 174–177 (2012).
[12] D. R. Lide, *CRC handbook of chemistry and physics*, Vol. 85 (CRC press, 2004).
[13] A. D. Rakić, A. B. Djurišić, J. M. Elazar, and M. L. Majewski, "Optical properties of metallic films for vertical-cavity optoelectronic devices," Appl. Opt. **37**, 5271–5283 (1998).
[14] J. I. Larruquert, A. P. Pérez-Marín, S. García-Cortés, L. Rodríguez-de Marcos, J. A. Aznárez, and J. A. Méndez, "Self-consistent optical constants of SiC thin films," J. Opt. Am. A **28**, 2340–2345 (2011).
[15] L. A. Bloomfield, *How Things Work: The Physics of Everday Life*, 5th ed. (Wiley, 2013).
[16] F. Reif, *Fundamentals of Statistical and Thermal Physics* (Waveland Press, 2009).
[17] K. Krishnakumar, "Micro-genetic algorithms for stationary and non-stationary function optimization," in *1989 Advances in Intelligent Robotics Systems Conference* (International Society for Optics and Photonics, 1990) pp. 289–296.
[18] D. E. Goldberg and K. Deb, "A comparative analysis of selection schemes used in genetic algorithms," Foundations of Genetic Algorithms **1**, 69–93 (1991).
[19] K. Deb and S. Agrawal, "Understanding interactions among genetic algorithm parameters," Foundations of Genetic Algorithms **5**, 265–286 (1999).
[20] J. M. Johnson and V. Rahmat-Samii, "Genetic algorithms in engineering electromagnetics," IEEE Antennas Propag. Mag. **39**, 7–21 (1997).
[21] C. H. Granier, F. O. Afzal, C. Min, J. P. Dowling, and G. Veronis, "Optimized aperiodic highly directional narrowband infrared emitters," J. Opt. Soc. Am. B **31**, 1316–1321 (2014).
[22] C. H. Granier, F. O. Afzal, S. G. Lorenzo, M. Reyes, Jr., J. P. Dowling, and G. Veronis, "Optimized aperiodic multilayer structures for use as narrow-angular absorbers," J. Appl. Phys. **116**, 243101 (2014).
[23] S. G. Johnson, "The NLopt nonlinear-optimization package," (2014).
[24] A. D. Simard, N. Belhadj, Y. Painchaud, and S. LaRochelle, "Apodized silicon-on-insulator Bragg gratings," IEEE Photon. Technol. Lett. **24**, 1033–1035 (2012).
[25] F. Bridou, F. Delmotte, Ph. Troussel, and B. Villette, "Design and fabrication of X-ray non-periodic multilayer mirrors: Apodization and shaping of their spectral response," Nucl. Instrum. Methods Phys. Res., Sect. A **680**, 69–74 (2012).
[26] G. A. Slack and S. Bartram, "Thermal expansion of some diamondlike crystals," J. Appl. Phys. **46**, 89–98 (1975).